**Atmospheric
Chemistry
and Physics**

The zonal structure of tropical O_3 and CO as observed by the Tropospheric Emission Spectrometer in November 2004 – Part 1: Inverse modeling of CO emissions

D. B. A. Jones[1], K. W. Bowman[2], J. A. Logan[3], C. L. Heald[4], J. Liu[1], M. Luo[2], J. Worden[2], and J. Drummond[1]

[1]Department of Physics, University of Toronto, Toronto, Ontario, Canada
[2]Jet Propulsion Laboratory, California Institute of Technology, Pasadena, California, USA
[3]School of Engineering and Applied Sciences, Harvard University, Cambridge, Massachusetts, USA
[4]Department of Atmospheric Science, Colorado State University, Fort Collins, CO, USA

Abstract. We conduct an inverse modeling analysis of measurements of atmospheric CO from the TES and MOPITT satellite instruments using the GEOS-Chem global chemical transport model to quantify emissions of CO in the tropics in November 2004. We also assess the consistency of the information provided by TES and MOPITT on surface emissions of CO. We focus on the tropics in November 2004, during the biomass burning season, because TES observations of CO and O_3 and MOPITT observations of CO reveal significantly greater abundances of these gases than simulated by the GEOS-Chem model during that period. We find that both datasets suggest substantially greater emissions of CO from sub-equatorial Africa and the Indonesian/Australian region than in the climatological emissions in the model. The a posteriori emissions from sub-equatorial Africa based on TES and MOPITT data were 173 Tg CO/yr and 184 Tg CO/yr, respectively, compared to the a priori of 95 Tg CO/yr. In the Indonesian/Australian region, the a posteriori emissions inferred from TES and MOPITT data were 155 Tg CO/yr and 185 Tg CO/yr, respectively, whereas the a priori was 69 Tg CO/yr. The differences between the a posteriori emission estimates obtained from the two datasets are generally less than 20%. The a posteriori emissions significantly improve the simulated distribution of CO, however, large regional residuals remain, and are likely due to systematic errors in the analysis. Reducing these residuals and

improving the accuracy of top-down emission estimates will require better characterization of systematic errors in the observations and the model (chemistry and transport).

1 Introduction

Atmospheric carbon monoxide (CO) is a product of incomplete combustion as well as a byproduct of the oxidation of atmospheric hydrocarbons. It plays a critical role in determining the oxidative capacity of the atmosphere as the primary sink of OH. Its abundance, therefore, influences the atmospheric lifetime of greenhouse gases, such as methane (CH_4), which are remove from the atmosphere through reaction with OH. Atmospheric CO is a precursor of tropospheric ozone (O_3) and, as a combustion product, provides a useful proxy for combustion-related emissions of other precursors of tropospheric O_3. Tropospheric O_3 is a harmfull pollutant and a greenhouse gas. Accurate and precise estimates of emissions of CO and other O_3 precursors are therefore important in both a climate and air quality context.

The Tropospheric Emission Spectrometer (TES) instrument is providing the first simultaneous, global, space-based observations of CO and O_3. We present here an analysis of the utility of inverse modeling of TES observations of atmospheric CO to better understand the impact of surface emissions of CO and O_3 precursors on the distribution of tropospheric CO and O_3. We focus on November 2004 when observations from TES revealed significantly higher abundances of atmospheric CO and O_3 in the southern tropics

than simulated by the GEOS-Chem chemical transport model (CTM). In the study presented here we focus on the inverse modeling of the CO observations. In a companion paper by Bowman et al. (2009) a detailed analysis is presented of the impact on tropical tropospheric O_3 of the changes in emissions of CO (and the implied changes in emissions of other O_3 precursors) inferred from the inversion analysis conducted here.

The dominant source of variability in atmospheric CO in the tropics is associated with biomass burning. Accurately quantifying emissions of CO from these sources is particularly challenging as they exhibit significant spatial and temporal variability and are sensitive to variations in the climate system such as the El Niño Southern Oscillation (ENSO) (Duncan et al., 2003; Van der Werf et al., 2004). For example, van der Werf et al. (2006) found that the standard deviation of the variability in the bottom-up estimates for carbon emissions biomass burning in Indonesia for 1997–2004 was 1.3 times as large as the mean emissions for the period. In late 2004 there was a weak El Niño in the tropical Pacific, which could account for some of the discrepancy between the model and observations. In our analysis we focus on quantifying the total combustion-related source of CO from different continental regions, with the assumptions that biomass burning is the dominant source of direct emissions of CO in the tropics and that interannual variability in biomass burning contributes largely to the discrepancy between the observations and the modeled CO distribution obtained with the climatological emission inventory.

In the past decade several inverse modelling studies of CO have been conducted using surface, aircraft, and satellite measurements (e.g. Bergamaschi et al., 2000a, b; Kasibhatla et al., 2002; Pétron et al., 2002, 2004; Palmer et al., 2003, 2006; Heald et al., 2004; Arellano et al., 2004, 2006; Müller and Stavrakou, 2005; Stavrakou and Müller, 2006; Kopacz et al., 2009). These studies have all produced different "top-down" estimates of the regional sources of CO (see discussion in Duncan et al., 2007), reflecting differences in inversion frameworks, atmospheric models (e.g. Arellano and Hess, 2006), and differences in the datasets employed in the analyses. A particular challenge for the earlier inversion analyses, which employed surface or aircraft measurements, was the limited spatial and temporal coverage provided by the observations. The recent satellite measurements of atmospheric CO, on the other hand, offer significantly greater spatio-temporal coverage and therefore provide more reliable constraints on regional surface emissions of CO (Heald et al., 2004). The Measurement Of Pollution In The Troposphere (MOPITT) instrument, launched in December 1999, provided the first continuous global measurements of atmospheric CO. A second objective of this study is to evaluate the consistency of the top-down constraints on surface emissions of CO provided by observations from TES and MOPITT.

The broad range of published top-down estimates of regional CO emissions reflects the fact that Bayesian inverse modeling is sensitive to systematic errors in the inverse models. Another objective of this study is to demonstrate that, despite the significantly increased spatio-temporal coverage offered by data from TES and MOPITT, the CO source estimates inferred from these datasets are sensitive to the presence of systematic errors. For example, Müller and Stavrakou (2005) showed that neglecting the non-linearity in the atmospheric chemistry of CO is an important source of systematic error in an inverse modeling analyses of atmospheric CO. Inversion studies typically prescribe abundances of atmospheric OH to account for the chemical sink of CO. However, if large changes in emissions of CO, such as those associated with enhanced biomass burning, are required in an inverse model to accommodate observations of CO, then there should be a concomitant increase in the model of emissions of O_3 precursors such as nitrogen oxides (NO_x), CH_4, and non-methane hydrocarbons (NMHC), which will, in turn, perturb the atmospheric abundance of OH. We examine here the potential feedback of perturbations in the atmospheric abundance of OH associated with changes in biomass burning on the atmospheric abundance of CO.

In Sect. 2 we begin with a brief description of the CO profile retrievals from the TES and MOPITT instruments. We describe the inversion methodology in Sect. 3. A description of the GEOS-Chem model is presented in Sect. 4, followed by a discussion of the inversion results in Sect. 5. In Sect. 6 we provide a summary of the results and a discussion of their implications for future inversion analyses of atmospheric CO.

2   The MOPITT and TES instruments

2.1   MOPITT

The MOPITT instrument (Drummond and Mand, 1996) was launched on 18 December 1999 on NASA's Terra spacecraft in a sun-synchronous polar orbit at an altitude of 705 km with an equator crossing time of 10:30 a.m. local time. It is gas correlation radiometer that measures thermal emission in the 4.7 μm region of the spectrum and has a spatial resolution of 22 km$\times$22 km. The MOPITT observation strategy consists of a 612 km cross-track scan that provides high data density; the instrument achieves nearly complete global coverage every 3 days.

Vertical profiles of CO are retrieved from the radiance measurements using an optimal estimation approach, described by Deeter et al. (2003). The retrieved mixing ratios are reported on 7 altitude levels, from the surface to 150 hPa. The data have been validated by inter-comparison with aircraft and other in-situ measurements (Emmons et al., 2004, 2007). In our analysis we employ version 3 MOPITT data and use profiles between 700–250 hPa, as these are the levels with most of the information in the retrievals (Emmons et

al., 2007). The retrieved profiles can be expressed as a linear estimate of the true atmospheric state

$$\hat{x}^{\mathrm{MOP}} = x_a^{\mathrm{MOP}} + \mathbf{A}^{\mathrm{MOP}}(x^{\mathrm{true}} - x_a^{\mathrm{MOP}}) + \varepsilon \tag{1}$$

where x_a^{MOP} is the MOPITT a priori CO profile, x^{true} is the true atmospheric state vector, $\mathbf{A}^{\mathrm{MOP}}$ is the MOPITT averaging kernel matrix, and ε is the measurement error. The averaging kernel is given by $\mathbf{A} = \partial \hat{x}^{\mathrm{MOP}} / \partial x^{\mathrm{true}}$ and represents the sensitivity of the MOPITT retrieval to the true state of the atmosphere and provides a measure of the vertical resolution of the retrieval.

2.2 TES

The TES instrument is a high resolution Fourier transform spectrometer that was launched on the Aura spacecraft on 15 July 2004. It measures thermal emission between 3.3–15.4 μm in both nadir and limb modes (Beer et al., 2001). The satellite is in a sun-synchronous orbit at an altitude of 705 km with an inclination of 98.2° and a repeat cycle of 16 days. The instrument operates in two observational modes: a global survey mode in which the observations are spaced about 5° along the orbit track, and a step-and-stare mode in which the observation are made every 40 km long the orbit. The horizontal resolution of the nadir observations is 8 km×5 km. Similar to MOPITT, vertical profiles of CO are retrieved from radiance measurements in the 4.7 μm spectral region using an optimal estimation approach. The TES retrievals, however, are performed for the logarithm of the mixing ratio of CO. A detailed discussion of the TES retrievals is given in Bowman et al. (2006). As for MOPITT, the TES retrievals can be expressed as a linear representation of the true atmospheric state

$$\hat{x}^{\mathrm{TES}} = x_a^{\mathrm{TES}} + \mathbf{A}^{\mathrm{TES}}(x^{\mathrm{true}} - x_a^{\mathrm{TES}}) + \varepsilon \tag{2}$$

where x_a^{TES} is the TES a priori CO profile, $\mathbf{A}^{\mathrm{TES}}$ is the TES averaging kernel matrix, and ε is the measurement error. For consistency with the inversion using MOPITT data, we restrict the TES profiles ingested in the inversion to between 800–250 hPa.

We employ 6 global surveys of TES CO data that were obtained during 4–16 November 2004. There were a limited number of global survey data available before and after this period in fall 2004. We use version V001 of the TES data as the major change in V002 was associated with improvements in the calibration algorithms to reduce biases in the TES radiances, which decreased the bias in the TES O$_3$ retrievals in the upper troposphere (Worden et al., 2007). The most significant change in the TES CO product occurred as a result of the warm-up of the optical bench in the instrument in December 2005 to correct for decreasing signal strength in the 1A1 filter. Before warm-up the sensitivity of the TES CO retrievals had dropped to less than 1 degree of freedom for signal (DOFS) compared to a sensitivity of 1–2 DOFS after launch and after the warm-up. The DOFS is the trace

of the averaging kernel matrix and provides a measure of the number of independent pieces of information on the vertical distribution of CO available in the retrieved profile. It is, in part, because of the low DOFS in the CO retrievals in 2005 that we restrict our analysis to fall 2004.

The TES and MOPITT CO data for early November 2004 are shown in Fig. 1. In general, the CO abundances retrieved from MOPITT radiances are greater in the Southern Hemisphere and lower in the Northern Hemisphere than those retrieved from TES because of the uniform a priori CO profile and constraint matrix used in the MOPITT retrievals (Luo et al., 2007a). In contrast, TES uses regionally varying a priori profiles and constraint matrices based on simulations from the MOZART model. A detailed comparison of the TES and MOPITT profile retrievals of CO was presented by Luo et al. (2007a), while validation of the TES CO retrievals with aircraft observations was conducted by Luo et al. (2007b). Luo et al. (2007a) found that despite the differences in the measurement and retrieval techniques of TES and MOPITT, both datasets provide about 0.5–2 DOFS in the troposphere. Luo et al. (2007a) found that after accounting for the a priori profiles incorporated in the retrievals and differences in the averaging kernels between the instruments the two datasets were in good agreement, with an absolute mean difference of less than 5% in the column abundances of CO. In the vertical profiles, the largest mean differences between the two datasets were −4.8% at 150 hPa (for TES compared to MOPITT), whereas the smallest mean differences were −0.2% at 850 hPa (Luo et al., 2007a). The focus of the work presented here is to assess if this agreement between the two datasets imply consistency in the constraints that they provide on surface emissions of CO when the data are incorporated in an inverse model.

3 Inversion methodology

The inversion framework employed here is described in Jones et al. (2003). We obtain optimized estimates of the sources of CO by minimizing the cost function (Rodgers, 2000)

$$J(\boldsymbol{u}) = (\hat{x} - F(\boldsymbol{u}))^T \mathbf{S}_\varepsilon^{-1}(\hat{x} - F(\boldsymbol{u})) + (\boldsymbol{u} - \boldsymbol{u}_a)^T \mathbf{S}_a^{-1}(\boldsymbol{u} - \boldsymbol{u}_a) \tag{3}$$

where $\hat{x}$ is the observation vector that consists of the retrieved vertical profiles of CO (defined in Eqs. 1 and 2 for MOPITT and TES, respectively), $\boldsymbol{u}$ is the state vector with elements representing the source regions shown in Fig. 2, and $\boldsymbol{u}_a$ is the a priori state vector, which is based on the emission inventory described in Sect. 4 and is given in Table 1. $\mathbf{S}_\varepsilon$ is the error covariance matrix of the observation vector and $\mathbf{S}_a$ is the a priori covariance matrix. Note, for consistency with the description of the satellite retrievals in Eqs. (1) and (2), we denote the state vector in the source inversion as $\boldsymbol{u}$ although the standard optimal estimation nomenclature as described in Rodgers (2000) uses $\boldsymbol{x}$ as the state vector.
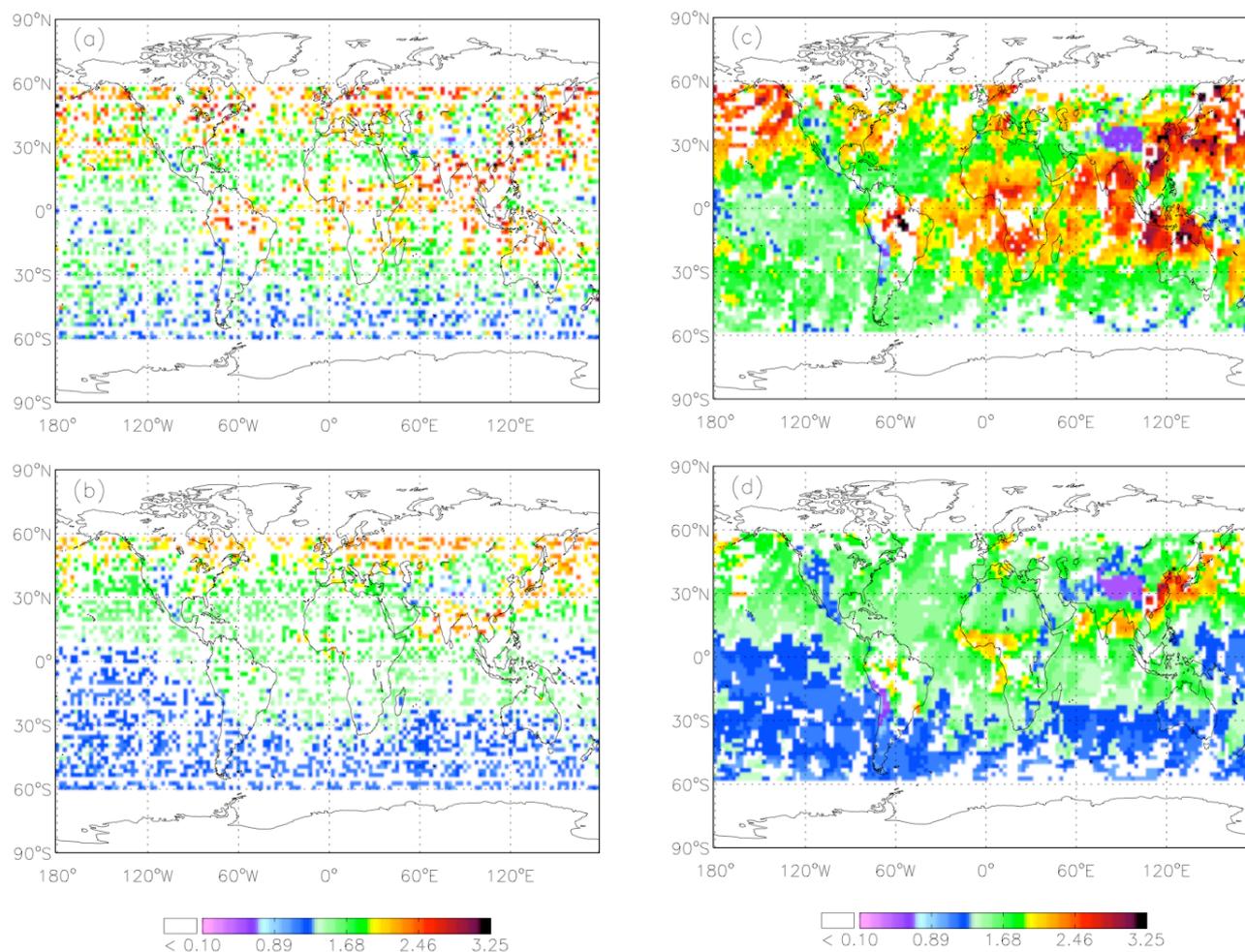
Fig. 1. **(a)** Column abundances of CO (in 10^{18} molecules cm^{-2}) from TES, averaged 4–15 November 2004. **(b)** Column abundances of CO from the GEOS-Chem model. The modeled fields were sampled along the TES orbit and smoothed using the TES averaging kernels and a priori profile. White areas are regions without observations. **(c)** Column abundances of CO (in 10^{18} molecules cm^{-2}) from MOPITT, averaged 5–15 November 2004. **(d)** Column abundances of CO from the GEOS-Chem model. The modeled fields were sampled along the MOPITT orbit and smoothed using the MOPITT averaging kernels and a priori profile. White areas are regions without observations.

The observation vector $\hat{\boldsymbol{x}}$ consists of 3011 and 10 613 profiles for the inversions with TES and MPOITT data, respectively. The MOPITT data were sampled on alternating days to match the one-day-on, one-day-off observational cycle of the TES global surveys. The forward model $F(\boldsymbol{u})$ reflects the transport of the CO emissions in the GEOS-Chem model, and accounts for the vertical sensitivity of TES and MOPITT and the a priori CO profile used in the retrievals in the two datasets. It is given by

$$\boldsymbol{F}^{\mathrm{MOP}}(\boldsymbol{u})=\boldsymbol{x}_a^{\mathrm{MOP}}+\mathbf{A}^{\mathrm{MOP}}(H(\boldsymbol{u})-\boldsymbol{x}_a^{\mathrm{MOP}}) \qquad (4)$$

and

$$\boldsymbol{F}^{\mathrm{TES}}(\boldsymbol{u})=\boldsymbol{x}_a^{\mathrm{TES}}+\mathbf{A}^{\mathrm{TES}}(ln[H(\boldsymbol{u})]-\boldsymbol{x}_a^{\mathrm{TES}}) \qquad (5)$$

where $H(\boldsymbol{u})$ is the GEOS-Chem model which transports and chemically transforms the CO emissions ($\boldsymbol{u}$).

We assume Gaussian error statistics for the observation and a priori errors, which yields the following maximum a posteriori (MAP) solution for the minimization of the cost function (Rodgers, 2000),

$$\boldsymbol{u}_{i+1}=\boldsymbol{u}_i+(\mathbf{K}_i^T \mathbf{S}_{\boldsymbol{\varepsilon}}^{-1}\mathbf{K}_i+\mathbf{S}_a^{-1})^{-1}\left[\mathbf{K}_i^T \mathbf{S}_{\boldsymbol{\varepsilon}}^{-1}(\hat{\boldsymbol{x}}-\boldsymbol{F}(\boldsymbol{u}_i))\right.$$
$$\left.-\mathbf{S}_a^{-1}(\boldsymbol{u}_i-\boldsymbol{u}_a)\right]. \qquad (6)$$

Here $\boldsymbol{u}_i$ and $\mathbf{K}_i=\partial\boldsymbol{F}(\boldsymbol{u}_i)/\partial\boldsymbol{u}$ are estimates of the state vector and the Jacobian matrix, respectively, at the i-th iteration. Note that the Jacobian accounts for the influence of the averaging kernels because of the definition of the forward model in Eqs. (4) and (5). Consequently, the difference in the vertical sensitivity of TES and MOPITT are incorporated into the inversion. It is necessary to use an iterative approach in solving for the MAP solution because of the slight

nonlinearity introduced by the logarithm in the TES forward model (Eq. 5). We obtain the solution in Eq. (6) using a Gauss-Newton method (Rodgers, 2000), with the sequential approach outlined in Jones et al. (2003). The Jacobian is estimated using a tagged CO approach, in which we specify separate atmospheric tracers of CO for emissions from each region in the state vector, as described in Sect. 4. The model was spun up starting in June 2003 and the Jacobian in November 2004, therefore, reflects the influence of emissions from previous months. Pétron et al. (2002), in their inversion analysis of CO, showed that the CO distribution in a given month has the greatest sensitivity to emissions from the preceding three months. The spin-up was performed to remove the influence of the initial conditions on the inversion, but the inversion was conducted for the dates in November 2004 as described in Sect. 2.

In constructing the a priori error covariance matrix we assume that emissions from the different sources are uncorrelated and have a uniform uncertainty of 50%, following Palmer et al. (2003), except for emissions from North American and Europe for which Palmer et al. (2003) assumed an uncertainty of 30%. We specify a uniform a priori constraint to more clearly assess the impact of the two datasets on the source estimates.

The observation error covariance matrix consists of the retrieval error covariance, the model error covariance, and the representativeness error covariance. Previous inverse modeling studies (Palmer et al., 2003; Jones et al., 2003; and Heald et al., 2004) for atmospheric CO have shown that the model error dominates the observation error covariance, with the representativeness and measurement errors providing a small contribution to the total error. In their inversion analysis of Asian emissions of CO, Heald et al. (2004) examined the sensitivity of the estimates of the CO sources to the specification of the model error. They compared the impact on the source estimates of specifying a uniform model error variance with that obtained using the complete model error covariance structure, as determined by Jones et al. (2003). Using the NMC method (Parrish and Derber, 1992) and pairs of 24-h and 48-h GEOS-Chem forecasts of CO, Jones et al. (2003) estimated the covariance error structure for the GEOS-Chem simulation of CO, which Heald et al. (2004) scaled based on the variance estimated from the difference statistics of the MOPITT data and the GEOS-Chem simulation. Heald et al. (2004) found that there was sufficient information in the MOPITT data such that the source estimates for regions with strong biomass burning emissions of CO, such as Southeast Asia, were insensitive to the specification of the error covariance structure. Assuming a uniform estimate of 20% for the total observation error in their analysis, for example, did not significantly influence the estimates for source regions such as Southeast Asia. In contrast, they found that the weaker regional sources, such as estimates for emissions from Western China and Japan and Korea were influenced strongly by the choice of error covariance. As our focus here
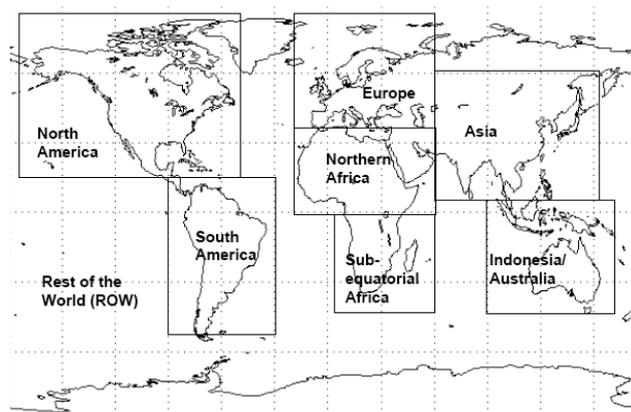

Fig. 2. Source regions comprising the state vector in the inversion analysis. The a priori estimates for emissions from these regions are listed in Table 1.

is on the dominant, continental-scale, biomass burning signals in the tropics, we assume a uniform observation error of 20%. This approach is similar to previous inverse modeling studies of CO such as Kasibhatla et al. (2002) and Pétron et al. (2002). We also neglect the correlations in the model error, but account for the influence of the averaging kernels from the instruments on the model error, which captures the vertical correlations associated with the vertical smoothing of the retrievals.

4 The GEOS-Chem model

The GEOS-Chem model (Bey et al., 2001) is a global three-dimensional CTM driven by assimilated meteorological observations from the NASA Goddard Earth Observing System (GEOS-4) from the Global Modeling and data Assimilation Office (GMAO). The meteorological fields have a horizontal resolution of $1° \times 1.25°$ with 55 levels in the vertical, and a temporal resolution of 6 h (3 h for surface fields). We employ version 7-02-04 of GEOS-Chem (http://www-as. harvard.edu/chemistry/trop/geos), with the resolution of the meteorological fields degraded to $2°$ latitude $\times 2.5°$ longitude. Recent applications of the model have been described in a range of studies (e.g. Suntharalingam et al., 2004; Heald et al., 2004; Park et al., 2005; Hudman et al., 2007; and Wang et al., 2007). The model includes a complete description of tropospheric O_3-NO_x-hydrocarbon chemistry, including the radiative and heterogeneous effects of aerosols.

The GEOS-Chem simulation of CO for 4–15 November 2004 is shown in Fig. 1. The model significantly underestimates the CO abundances as observed by TES and MOPITT, reflecting the climatological emission inventories used in the simulation. Anthropogenic emissions of CO in this version of GEOS-Chem are as described by Duncan et al. (2007), with emissions for the base year of 1985 in the inventory scaled to 1998. For biomass burning we employ

Table 1. A priori and a posteriori source estimates.

Region	A priori[a] (Tg CO/yr)				A posteriori TES 4–16 Nov (Tg CO/yr)	A posteriori MOPITT 5–15 Nov (Tg CO/yr)	A posteriori MOPITT 5–28 Nov (Tg CO/yr)	Difference between estimates from TES and MOPITT[c] (%)
	BB	BF	FF	Total				
North America	23	6	106	135 (21)[d]	36 (6)	146 (23)	165 (26)	−75
Europe	8	17	85	110 (19)	132 (23)	111 (19)	111 (19)	19
Asia	102	93	171	367 (50)	511 (70)	531 (72)	483 (66)	−4
South America	69	19	25	113 (25)	118 (26)	141 (31)	157 (35)	−16
Northern Africa	99	21	19	139 (16)	131 (15)	119 (14)	174 (20)	10
Sub-equatorial Africa	78	10	6	95 (20)	173 (36)	184 (39)	185 (39)	−6
Indonesia/ Australia	49	7	13	69 (18)	155 (40)	185 (48)	165 (43)	−16
Rest of the World[b]				1215 (195)	1390 (223)	1344 (216)	1336 (214)	3
Total				2243	2646	2761	2776	−4

[a] Sources represent emissions of CO from fossil fuel (FF) and biofuel combustion (BF) and biomass burning (BB), based on Duncan et al. (2003, 2007).

[b] The rest of the world source includes CO from the oxidation of methane and non-methane hydrocarbons.

[c] Difference in TES a posteriori estimates relative to those from MOPITT calculated from data in early November.

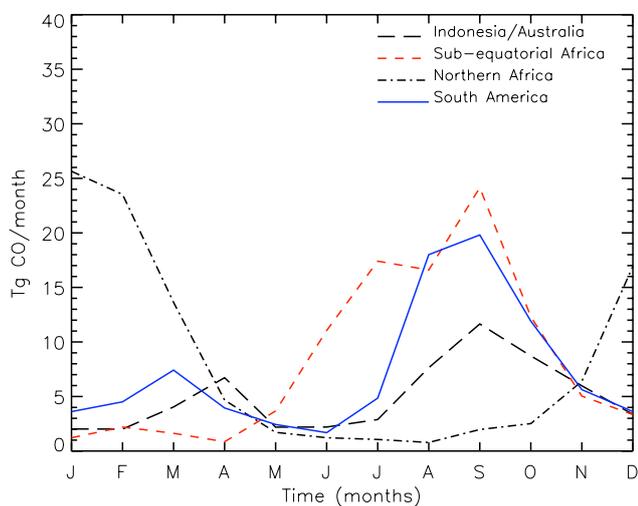[d] Values in parentheses represent the estimated source of CO for October and November 2004 in Tg CO.

Fig. 3. Seasonal variations of the a priori tropical biomass burning emissions employed in the GEOS-Chem model. The emissions have been aggregated for the regions defined in Fig. 2.

the emission inventory of Duncan et al. (2003), whereas for biofuel combustion we use estimates from Yevich and Logan (2003). The total a priori global emissions of CO, as well as the total secondary source of CO from the oxidation of methane and NMHC is given in Table 1. Shown in Fig. 3

are the seasonal variations of the total a priori emissions aggregated for the four tropical regions in our analysis. The model simulation of CO using the a priori emissions is compared in Fig. 4 with surface observations from the NOAA Earth System Research Laboratory (ESRL)/Global Monitoring Division (GMD) Carbon Cycle Greenhouse Gases network (http://www.esrl.noaa.gov/gmd/ccgg/index.html). As shown in Fig. 4, the model captures the seasonality of the surface data at the GMD observation sites. This is consistent with the results of Bian at al. (2007), who compared model simulations of CO obtained with the Duncan et al. (2003) biomass burning inventory with those based on the Global Fire Emissions Database (GFED) versions 1 and 2 inventory and the top-down biomass burning inventory of Arellano et al. (2006) and found that, although the inventories produced different regional biases in the simulated CO abundance, the modeled CO distributions were generally within the range of variability of CO observed at many of the sites in the GMD network.

In our inversion analysis we specify monthly mean concentrations of OH to linearize the chemistry of CO. This approach has been used previously for the inverse modeling of CO using the GEOS-Chem model (e.g. Palmer et al., 2003, 2006; Jones et al., 2003; Heald et al., 2004; and Kopacz et al., 2009). Linearization of the chemistry enables us to efficiently calculate the Jacobian in the inversion analysis by specifying a separate tracer for each region considered in the
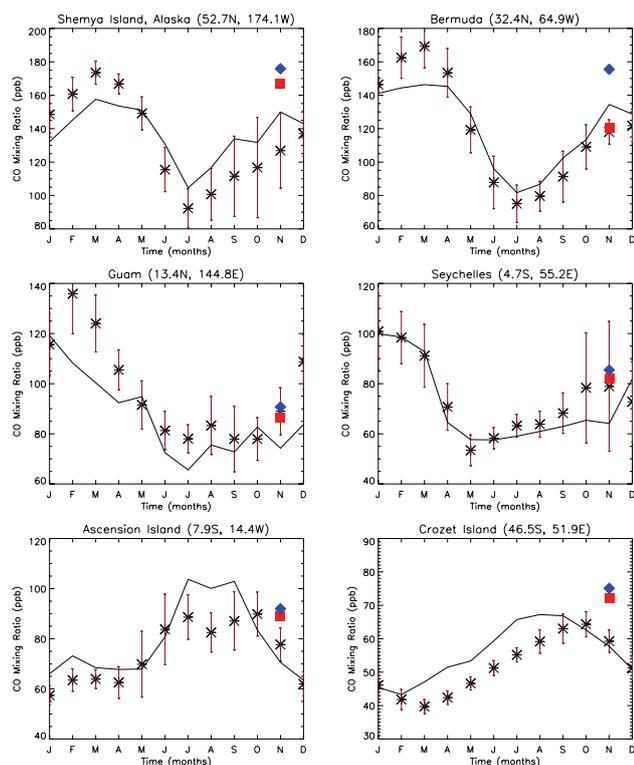
Fig. 4. Comparison of the GEOS-Chem simulation of CO with monthly mean surface observations of CO for 2004 from the GMD network. Asterisks represent GMD CO data with the 1-σ variability (for 1996–2004) indicated by the error bars. The model simulation with the a priori emissions is shown with the solid black line. The modeled CO for November 2004 with the a posteriori emissions estimated from TES and MOPITT data is denoted by the red square and the blue diamond, respectively.

state vector. These OH fields were obtained from an earlier version of the full chemistry simulation of GEOS-Chem (Evans and Jacob, 2005) and have a global annual mean OH abundance of $10.8 \times 10^5 \text{cm}^{-3}$.

5   Results

The results of the inversion analysis using data from TES and MOPITT for early November 2004 are shown in Fig. 5 and Table 1. They suggest significantly greater emissions of CO in sub-equatorial Africa and the Indonesian/Australian region than the a priori. In sub-equatorial Africa, where the a priori estimate is 95 Tg CO/yr (Table 1), the inferred emission estimate from TES data is 173 Tg CO/yr, while the estimate based on MOPITT data is 184 Tg CO/yr. In the Indonesian/Australian region the a posteriori emission estimates are 155 Tg CO/yr and 185 Tg CO/yr, based on the TES and MOPITT data, respectively, compared to the a priori of 69 Tg CO/yr. For comparison, the Global Fire Emissions Database version 2 (GFEDv2) emission inven-
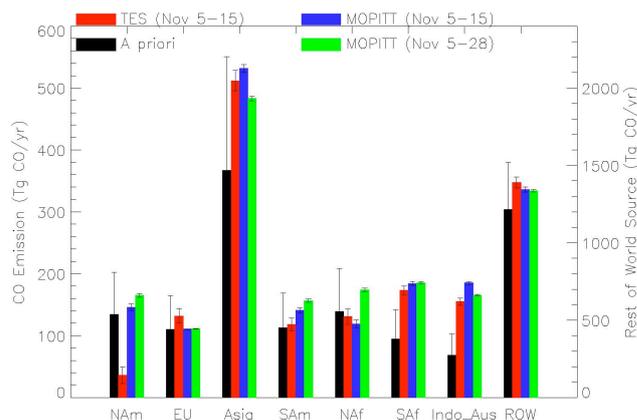

Fig. 5. A priori and a posteriori CO source estimates. Black bars indicate the a priori emission estimates, red bars are the a posteriori estimates inferred from TES data (4–15 November 2004), whereas the blue bars are the a posteriori estimates based on MOPITT data (5–15 November 2004). The green bars represent the a posteriori emission estimates obtained using MOPITT data for 5–28 November 2004. The regional definitions are: North America (NAm), Europe (EU), South America (SAm), North Africa (NAf), sub-equatorial Africa (SAf), Indonesia/Australia (Indo_Aus), and the rest of the world and the background chemical source of CO (ROW). The magnitude of the estimate for the ROW is indicated on the right y-axis. Error bars indicate an uncertainty of 1-σ.

tory (van der Werf et al., 2006) provides an a priori estimate of 78 Tg CO and 74 Tg CO for annual biomass burning emissions in 2004 from the Indonesian/Australian region and sub-equatorial Africa, respectively, which are much lower than our a posteriori estimates. van der Werf et al. (2006) noted the total global carbon emissions from biomass burning in the GFEDv2 inventory of 2.0 Pg C/yr, for April 2000–March 2001, was much lower than the estimate of 3.4 Pg C/yr inferred by Arellano et al. (2006) in their inversion analysis of MOPITT data. Following Palmer et al. (2003) and Heald et al. (2004) we assume here that the seasonality of the sources in the model (shown in Fig. 3) is correct and, therefore, report the source estimates as annual means although the inversion provides constraints on the source estimates mainly for the October to November period, due to the atmospheric lifetime of CO of weeks to a few months. In the analysis we do not attempt to discriminate between emissions of CO from different source types, such as biomass burning or fuel combustion. The globally averaged source of CO estimated from the TES and MOPITT measurements are 2646 Tg CO/yr and 2761 Tg CO/yr, respectively, compared to the a priori of 2243 Tg CO/yr (Table 1).

The a posteriori estimates of the CO emissions for sub-equatorial Africa and the Indonesian/Australian region based on the TES data thus represent an increase in emissions by a factor of 1.8 and 2.3, respectively, above the a priori values. The large increase in emissions from these regions are consistent with the results of Arellano et al. (2006), who

conducted an inversion analysis of MOPITT data for 2000–2001 and reported similarly greater top-down estimates of CO emissions. Arellano et al. (2006) estimated total a posteriori emissions from Indonesia and Oceania (which includes Australia) of about 165 Tg CO/yr, which is comparable to the estimates of 155–185 Tg CO/yr obtained in this study. For sub-equatorial Africa they reported an estimate of 203 Tg CO/yr, slightly larger than the 175–185 Tg CO/yr obtained here. It should be noted that in their analysis, Arellano et al. (2006) quantified separately CO emissions from fuel combustion and biomass burning and found that fuel combustion provided a significant contribution to the total a posteriori emission estimates for Indonesia and sub-equatorial Africa. For example, their a posteriori estimate for emissions from fuel combustion from Indonesia and Oceania were 84 Tg CO/yr and about 5 Tg CO/yr, respectively. In contrast, their a posteriori estimate for biomass burning from these regions was 76 Tg CO/yr. We do not believe that our inversion approach can reliably discriminate between emissions of CO from fuel combustion and biomass burning. However, the consistency between our results for 2004 and those of Arellano et al. (2006) for 2000 does suggest that fuel combustion may indeed be responsible for a large fraction of the emissions as these sources have less interannual variability.

In a companion paper by Bowman et al. (2009) the a posteriori emissions from the inversion are evaluated in the context of their impact on the modeled O_3 distribution. Using a forward model simulation of GEOS-Chem with the O_3 precursor emissions from fuel combustion and biomass burning scaled by the regional scaling factors obtained in the CO inversion, Bowman et al. (2009) showed that the a posteriori emissions provide an improved simulation of O_3 over Indonesia and Australia. Throughout the free troposphere over Indonesia and Australia O_3 increased in the model by as much as 10 ppb, reducing the maximum bias in the modeled O_3 distribution relative to TES by about 40%. In contrast, in the free troposphere over the tropical Southern Atlantic, Bowman et al. (2009) found that the improvement in the modeled O_3 with the a posteriori emissions was modest, despite the large increases in surface emissions from sub-equatorial Africa, reflecting the greater influence of NO_x from lightning on the budget of O_3 in this region.

The results obtained here show that TES and MOPITT data provide consistent constraints on surface emissions of atmospheric CO. As shown in Table 1, the absolute differences in the source estimates inferred from the two datasets are about 20% or less, with the exception of emissions from North America, which is discussed further below. These differences represent the potential influence on the source estimates of the different spatio-temporal sampling of the TES and MOPITT measurements when the data are incorporated into a regional Bayesian inverse analysis.

We conducted a sensitivity analysis using observations from MOPITT for 5–28 November to determine the potential impact on the source estimates of using only two week of data on early November. We found that the MOPITT data for 5–28 November data produced results similar to those obtained with data for the first half of November, with the exception of the North African emission estimates. This is consistent with the simulation experiments of Jones et al. (2003) that suggested two weeks of TES would provide sufficient information to quantify large-scale continental sources of CO.

We examined the correlation between the a posteriori estimates for the southern tropical sources and found that with both TES and MOPITT data the correlations between the source estimates were small ($r < 0.4$). The correlation coefficient was calculated using the expression

$$r_{ij} = \frac{\hat{S}_{ij}}{\sqrt{\hat{S}_{ii}}\sqrt{\hat{S}_{jj}}}, \tag{7}$$

where $\hat{S}_{ij}$ is the a posteriori covariance between the i-th and j-th elements of the state vector. The inversion analysis can independently quantify emissions from the three continental regions in the southern tropics because transport patterns from these regions are broad and are relatively distinct, reflecting the regional meteorology. The distribution of the tagged CO tracers emitted from South America, sub-equatorial Africa, and the Indonesian/Australian region are shown in Fig. 6. Emissions from South America are entrained into the subtropics in the southern tropical Atlantic and are transported eastward in the westerlies in the subtropics and extratropics of the Southern Hemisphere. Emissions from sub-equatorial Africa, on the other hand, are exported across the Indian Ocean and Australia. Over Australia and Indonesia the dominant contribution to the total abundance of CO in the free troposphere is from local emissions convectively transported out of the boundary layer. Gloudemans et al. (2006) also showed that long-range transport of emissions from South America and sub-equatorial Africa also contribute to CO abundances over Australia. In general, over each continental region, convective transport of surface emissions to the upper troposphere and subsequent eastward outflow provides a strong signal for CO in the middle troposphere where TES and MOPITT are most sensitive.

While the focus on this analysis is on the tropics, the inverse model is global in scope and the major discrepancy between the results obtained with TES data and those from MOPITT data is in the estimate for North American emissions. The TES data suggest a significantly reduced North American source of CO compared to the a priori, whereas the MOPITT data suggest a slightly larger source (Table 1). Recently, Hudman et al. (2008) suggested that a 60% reduction in anthropogenic emissions in North America, relative to the US EPA NEI99 inventory is required to reconcile the model simulation of CO with aircraft observations of
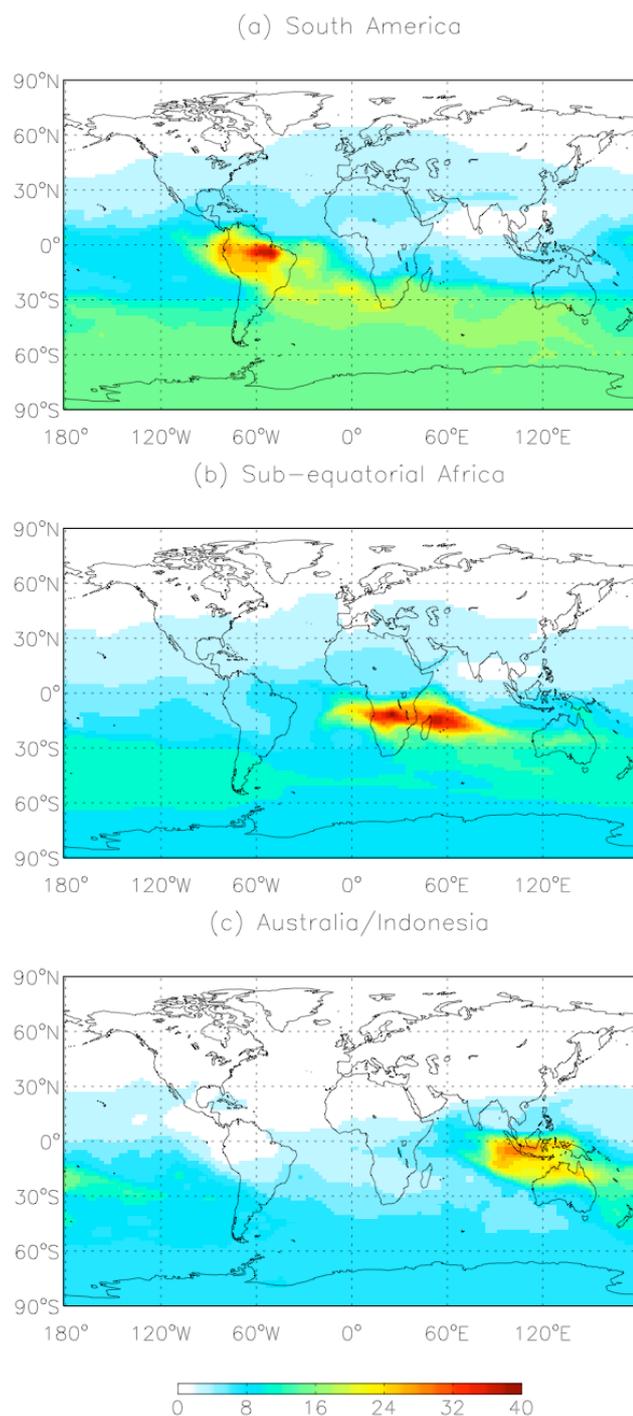
Fig. 6. Distribution of the tagged CO tracer for emissions of **(a)** South America, **(b)** sub-equatorial Africa, and **(c)** Indonesia/Australia. The tracer distributions were obtained using the a priori CO emissions and are shown as a percentage of total CO at about 8 km, averaged between 1–15 November 2004.

CO from the ICARTT campaign. The reduction of the estimate of the North American source with the TES data seems to be consistent with the recommendation of Hudman et
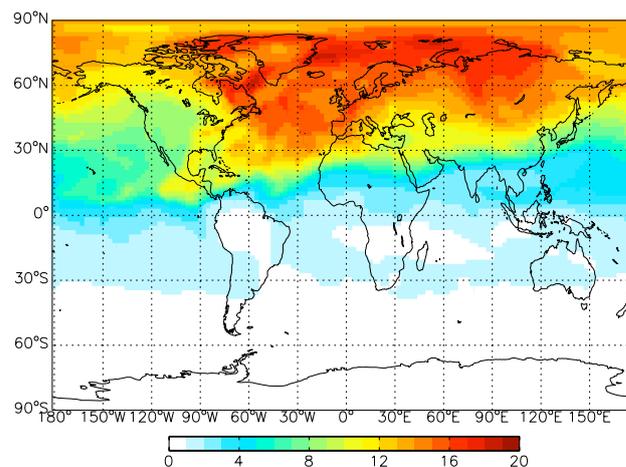

Fig. 7. Contribution of emissions of CO from North America (as defined in Fig. 2) to the total abundance of CO. The tracer distribution, as a percentage of total CO, is shown averaged between 1–15 November 2004 at about 8 km.

al. (2008). However, we do not believe that the inversion provides a reliable estimate of the North American emissions. We found that with TES data the North American source estimate is correlated with the European estimate ($r=-0.6$). With MOPITT data, however, the North American and European source estimates are uncorrelated ($r=-0.09$). The challenge with quantifying the North American emissions is that in boreal fall these emissions provide a small contribution to the total CO abundance in the free troposphere at midlatitudes. As shown in Fig. 7, North American emissions account for less than about 20% of the total CO in the middle troposphere at midlatitudes, which means that the signal for North American emissions is more challenging to discriminate from the background, given the noise level in the inversion analysis. In contrast, in Jones et al. (2003) two weeks of pseudo-data from TES in March were sufficient to quantify emissions from North America, Europe, and Asia because emissions from these regions provided a larger contribution to the total CO abundance as a result of the longer atmospheric lifetime of CO in spring.

The difference in the North American source estimates obtained with TES and MOPITT data may be due to the fact that there are episodic transport events, such as warm conveyor belts associated with the passage of cold fronts, which transport air out of the North American boundary layer and produce enhanced levels of CO in the free troposphere. These signals are localized spatially and temporally and are therefore not easily captured by the TES data. MOPITT, on the other hand, because of its greater spatio-temporal sampling density can resolve these synoptic structures (Liu et al., 2006) and therefore may provide more constraints on North American emissions.

The discrepancy between the North American estimates illustrates the importance of properly selecting the state vector in the inversion analysis that is consistent with the spatio-temporal sampling of the observation used in the analysis. Ideally, the estimates for those elements of the state vector for which the observations provide little information should remain at the values specified by the a priori. The low estimate of the North American source obtained with the TES data indicate the presence of systematic errors in the inverse model.

The results obtained using both TES and MOPITT data suggest significantly larger emissions from Asia, 511 Tg CO/yr and 531 Tg CO/yr, respectively, compared to the a priori estimate of 367 Tg CO/yr. In contrast, the inverse modeling studies of Heald et al. (2004) and Arellano et al. (2006), which inferred CO emissions from MO-PITT data, reported estimates for the Asian emissions of CO (excluding emissions from Indonesia) of 282 Tg CO/yr and 402 Tg CO/yr, respectively. The differences between the a posteriori estimates of the Asian sources reported by these studies are due, in part, to the fact that these studies used different inversion configurations. Heald et al. (2004) conducted a regional inversion analysis for Asia, whereas Arellano et al. (2004) performed a global analysis. In addition, the analyses were focused on different periods: our analysis was carried out for November 2004, whereas the Heald et al. (2004) study was focused on February–April 2001, and Arellano et al. (2006) conducted a time dependent inversion analysis for April 2000–April 2001. These studies will, therefore, be impacted differently by the spatio-temporal sampling of the data and by systematic errors associated with the transport and chemistry. It is also possible that some fraction of the differences between the Asian estimates reported here and those from the earlier studies could reflect actual increases in emissions of CO in Asia since 2000. However, examination of the residuals from the CO simulation with the a posteriori emissions (discussed below), show that the Asian estimates reported here do provide an overestimate of the Asian sources of CO, suggesting that these emissions are not well constrained by the observations. This is likely due to the fact that the contribution of direct Asian emissions to the total atmospheric abundance of CO is small in summer and fall compared to winter and spring. This low sensitivity combined with the presence of systematic errors in the inversion (in either the data or the model) could adversely impact the source estimates.

As mentioned above, the source estimates obtained from two weeks of MOPITT data are consistent with those inferred from data for the whole month of November 2004. The exception is for north equatorial Africa, for which the inversion using the latter dataset suggests a much larger estimate for the CO emissions compared to results with the former. Biomass burning, which is the dominant source of CO from north equatorial Africa, increases during boreal fall and winter, reaching a maximum in December–January (Duncan et al., 2003). Indeed, fire-counts inferred from the MODIS instrument show more widespread burning in late November 2004, compared to early November. This increased burning later in the month is reflected in the larger source estimate obtained when MOPITT data from late November is included in the inversion analysis.

5.1 Comparison of GEOS-Chem with a posteriori emissions to TES and MOPITT

The a posteriori emissions provide a significantly improved simulation of the distribution of CO, as shown in Table 2 and Figs. 8 and 9. The global mean bias (averaged 60° S–60° N) in the modeled column abundances of CO with respect to the TES data is reduced from -12% to 0.1%, while the bias with respect to the MOPITT data is reduced from -22% to -0.8%. Despite the significant improvement in the global mean CO, the model simulation with the optimized emissions produces large regional biases, as shown in Figs. 8, 9, and Table 2. The residuals of the model fit to the TES and MOPITT data shown in Figs. 8b and 9b and Table 2 indicate that the inversion with both datasets provides an underestimate of 3–7% of the CO column abundances over the southern tropical Atlantic, Southern Africa, and over the Indian Ocean.

The optimized emissions inferred from MOPITT data produce an underestimate of CO abundances over the Sahara, the Middle East, and over the North Pacific, while they result in an overestimate of CO abundances across the tropical Pacific and over tropical Western Africa. These regional biases, however, are compensatory such that the mean bias across the tropics and midlatitudes of the Southern Hemisphere (0°–45° S) is small, -3% and -1% for emissions inferred from TES and MOPITT data, respectively. Similarly, in the extratropics of the Northern Hemisphere (25°–60° N) the mean biases in the model, relative to the TES and MOPITT data, are reduced from -7% and -18%, respectively, to 0.9% and -2.7% with the a posteriori emissions. The fact that the reduced North American emissions obtained with the TES data do not contribute to a noticeable bias between the model simulation with the a posteriori emissions and the TES observations over North America is an indication that, as discussed above, North American emissions provide a small contribution to the total CO in the free troposphere in boreal fall.

The large a posteriori estimate for Asian emissions represents an overestimate of the Asian sources, as reflected in the large positive residuals over East Asia (Figs. 8b and 9b and Table 2). As mentioned above, this is likely due to a combination of aggregation errors in the inversion analysis and bias in the model transport or chemical fields. With the a priori emissions, the model underestimates the CO abundance over the North Pacific compared to the observations from TES and MOPITT. Emissions of CO from Southeast Asia represent a large contribution to the total CO in the upper troposphere over the Pacific. The a priori bias over the North

Table 2. Regional bias in the model simulation of CO[a].

	TES		MOPITT	
Region	A priori bias (%)	A posteriori bias (%)	A priori bias (%)	A posteriori bias (%)
Globe (60° S–60° N)	−12	0.1	−22	−0.8
Southern Hemisphere (0°–45° S)	−18	−2	−27	−1
Southern Atlantic (35°–0° S, 40° W–5° E)	−18	−3	−27	−5
Southern Africa/Indian Ocean (35°–15° S, 15°–90° E)	−20	−5	−31	−7
Central Pacific Ocean (10° S–10° N, 180° W–80° W)	−14	0.3	−13	8
Northern Hemisphere (25° N–60° N)	−7	1	−18	−3
North Pacific (25°–60° N, 175° W–120° W)	−10	−0.9	−24	−8
East Asia (25°–60° N, 110° E–135° E)	−4	3	−12	6

[a] The bias is calculated (model minus observations) with respect to CO columns from TES and MOPITT data, with the a priori and a posteriori emissions of CO in the model.

Pacific could reflect either an underestimate in the magnitude of these emissions or a bias in the rate at which these emissions are transported to the upper troposphere (mostly likely by convective transport). By aggregating all of the Asian emissions into one region, the inversion analysis scales all of the Asian emissions in trying to compensate for this underestimate of CO over the North pacific, potentially resulting in an overestimate of the Eastern Asian emissions. As demonstrated recently by Kopacz et al. (2009), conducting the inversion at the resolution of the model would provide maximum flexibility in adjusting the emissions to best reproduce the observations (given the uncertainty of the observations and the model simulation), while minimizing the aggregation errors.

The model simulations with the a posteriori emissions are compared with surface observations from the GMD network in November 2004 in Fig. 4. At the Seychelles and Guam, in the Indian and Pacific Oceans, respectively, the a posteriori emissions provide a significantly improved simulation of the observations in November 2004. At the Seychelles the bias was reduced from −14.8 ppb to 3.2 ppb and 6.5 ppb with the TES and MOPITT a posteriori inventories, respectively, whereas at Guam it was reduced from −14.7 ppb to −2.4 ppb and 1.7 ppb for TES and MOPITT, respectively. At Ascension Island and in the midlatitudes of the Southern Hemisphere both a posteriori emissions result in a significant overestimate of the observed CO abundances (the bias increased from −7.1 ppb to 11.3 ppb and 14.3 ppb for TES and MOPITT). The overestimate of CO in these regions was

noted by Arellano et al. (2006) in their inversion analysis of the MOPITT data. They speculated that the discrepancy at Ascension Island could be due to a bias in the altitude dependence of the model transport. Similarly, the positive bias in the CO simulation at Crozet Island with the a posteriori estimates from both datasets suggests a possible bias in the model transport of CO to the free troposphere of the mid-altitudes of the Southern Hemisphere.

At Shemya Island, in the Northern Hemisphere, both a posteriori inventories produce an overestimate of the observed CO, which may be due to the overestimate of the Asian emissions in the inversion. At Bermuda, the TES-derived emissions correct the positive bias in the a priori simulation of CO in the model, whereas the MOPITT-derived emissions exacerbated the positive bias. The apparent improvement in the model simulation at Bermuda with the TES data is due to the significant reduction in North American emissions obtained with TES data. This suggests that both datasets may provide poor constraints on North American emissions in fall. However, as we noted above, recent work by Hudman et al. (2008) suggests that a 60% reduction in anthropogenic emissions in North America is required to reconcile the model simulation of CO with aircraft observations from the ICARTT campaign. The agreement between the model and the surface observations at Bermuda would support that recommended reduction, but as we noted above, the inversion with TES data cannot independently quantify North American and European emissions.
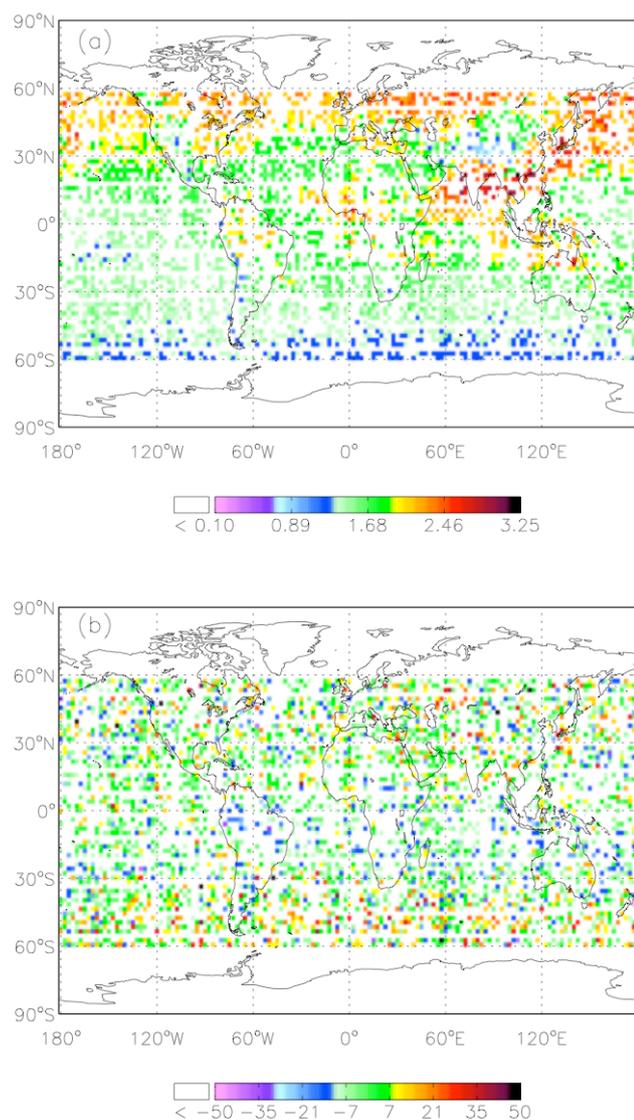
Fig. 8. (a) Column abundances of CO, averaged from 4–15 November 2004, from the GEOS-Chem simulation of the a posteriori emissions. Modeled fields transformed using the TES averaging kernels and a priori profiles. Units are 10^{18} molecules cm^{-2}. **(b)** The residuals expressed as a percent difference between the model and the TES observations (model minus TES). The TES data are shown in Fig. 1.

Fig. 9. (a) Column abundances of CO, averaged from 5–15 November 2004, from the GEOS-Chem simulation of the a posteriori emissions. Modeled fields transformed using the MOPITT averaging kernels and a priori profiles. Units are 10^{18} molecules cm^{-2}. **(b)** The residuals expressed as a percent difference between the model and the MOPITT observations (model minus MOPITT). The MO-PITT data are shown in Fig. 1.

5.2 Feedback of changes in atmospheric OH on CO

In the inversion analysis we linearized the chemistry of CO by imposing monthly mean concentrations of OH, the main sink for atmospheric CO. This, however, introduces biases in the inversion as observations of CO ingested in the analysis will also reflect the influence of OH concentrations characteristic of different background chemical conditions in the atmosphere. For example, enhanced emissions of CO in Indonesia/Australia, as suggested by the observations, will result in a reduction of atmospheric OH, which will have a
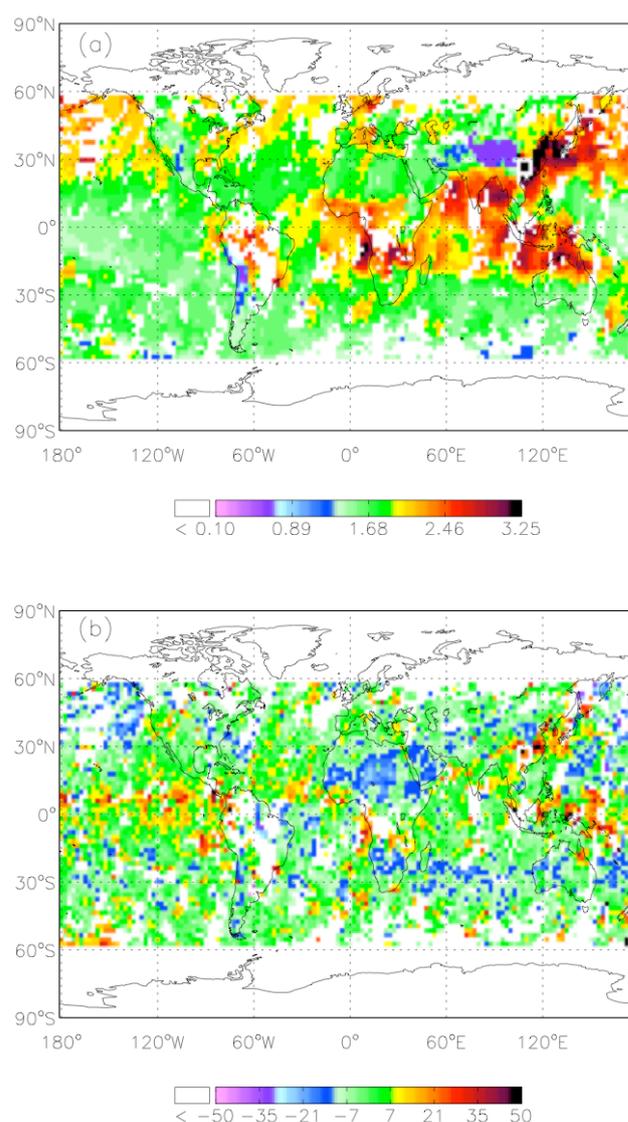
direct feedback on CO abundances. However, increases in combustion-related emissions of O_3 precursors will lead to elevated atmospheric abundances of O_3 and OH, and consequently to suppressed concentrations of CO. To assess the magnitude of this indirect feedback on the atmospheric concentrations of CO we conducted a forward model simulation with the full nonlinear chemistry and with the combustion-related emissions of NO_x (from biomass burning and biofuel and fossil fuel combustion) scaled uniformly according to the regional scaling factors obtained in the inversion analysis

of the CO data. We focus on changes in NO_x emissions as NO_x is a key O_3 precursor and the TES observations indicate that the model underestimates O_3 across the southern tropics (Bowman et al., 2009). We scale only NO_x emissions in the simulation and compare the resulting CO distribution with that obtained with the a priori NO_x emissions. We neglect possible errors associated with assuming that the relative contribution of different source types to the total emissions of NO_x is the same as for emissions of CO in these regions.

The change in the abundance of CO obtained with the scaled NO_x emissions is shown in Fig. 10. The increased emissions of NO_x from Indonesia and Australia results in a reduction of CO by as much as 7–10 ppb, corresponding to about 10% of the total CO abundance. This decrease in CO is a result of increased tropospheric O_3, and thus OH, in the Indonesian/Australian region. Higher concentrations of NO_x produce an increase in O_3 throughout the southern tropics, with the largest increases, of about 35%, in the middle/upper troposphere over Indonesian/Australian (not shown). A decrease of about 7–10 ppb in CO over Indonesia and Australia represents about 20–30% of the contribution of emissions from this region to the total abundance of CO (Fig. 6) and suggests that neglecting the chemical feedback of changes in surface emissions on the abundance of OH, and thus CO, could introduce biases in the a posteriori estimates of the sources of CO. Indeed, in their inversion analysis of surface measurements of CO and GOME observations of NO_2, Müller and Stavrakou (2005) found that using GOME NO_2 observations and the surface CO data together was better than using only the surface CO data. Their a posteriori CO emissions obtained by simultaneously optimizing the CO and NO_x sources provided a better simulation of independent aircraft observations of CO than those estimated from only the surface CO data.

6 Summary and discussion

We have conducted an inverse modeling analysis of observations of atmospheric CO from the TES and MOPITT satellite instruments to quantify emissions of CO in the tropics in November 2004 and to assess the consistency of the constraints that data from these instruments provide on estimates of surface emissions of CO. We focused our analysis on observations from November 2004, during the biomass burning season in the Southern Hemisphere, when observations from TES and MOPITT indicated that the climatological emissions inventory in the GEOS-Chem model significantly underestimated the abundance of CO observed by both instruments. We used a maximum a posteriori inverse modeling approach to quantify the magnitude of emissions of CO most consistent with the observations. Although our focus was on the tropics, the inversion analysis was global, employing profile retrievals of CO from MOPITT and TES between $60°$ S–$60°$ N.
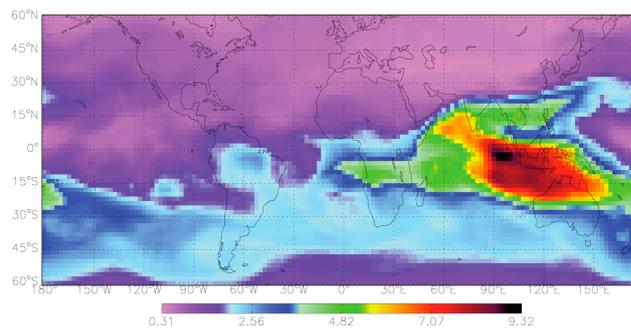

Fig. 10. Difference in modeled CO at 8 km in the GEOS-Chem model between simulations with the a priori emissions and with combustion related NO_x emissions scaled based on the regional scaling factors from the CO inversion. Shown are the differences in the distribution between the a priori minus scaled NO_x simulations, averaged between 1–15 November 2004. Units are ppb.

The TES and MOPITT data provided consistent information on the CO sources; differences between the a posteriori emission estimates obtained from the two datasets were generally less than 20%. We found that both datasets suggested significantly greater emissions of CO (by a factor of 2–3) from sub-equatorial Africa and from the Indonesian/Australian region in November 2004. The a posteriori emissions from sub-equatorial Africa based on TES and MOPITT data were 173 Tg CO/yr and 184 Tg CO/yr, respectively, compared to the a priori of 95 Tg CO/yr. In the Indonesian/Australian region, a posteriori emissions inferred from TES and MOPITT data were 155 Tg CO/yr and 185 Tg CO/yr, respectively, whereas the a priori was 69 Tg CO/yr. In contrast, the a posteriori emissions from South America were not significantly different from the a priori.

We found that while the source estimates for the TES and MOPITT were consistent, the inversion was less sensitive to the midlatitude sources in the Northern Hemisphere, because direct emissions of CO from these sources provide a smaller contribution to the total atmospheric CO in fall than in late winter and spring. The inversion produced much larger estimates for emissions from Asia, 511 Tg CO/yr based on TES data and 531 Tg CO/yr based on MOPITT data, which are greater than most previously published estimates of Asian emissions. These a posteriori emissions result in large residuals over East Asia, with the model simulation providing an overestimate of the observed CO from both TES and MOPITT, whereas the model simulation with the a priori emissions underestimated the observed CO over this region. The residual bias over East Asia is likely a result of systematic errors in the model chemistry and transport fields.

We also examined the feedback on atmospheric CO of variations in tropospheric OH associated with changes in biomass burning emissions, as suggested by the a posteriori CO source estimates. Using a forward model simulation

of the full tropospheric chemistry with NO_x emissions from combustion sources scaled uniformly based on the regional scaling factors inferred in the CO inversion analysis produced increases in O_3 and OH throughout the southern tropics with the largest increases over Indonesia/Australia. The abundance of O_3 increased by about 35% in the middle/upper troposphere over Indonesian/Australia. Bowman et al. (2009) show that the regional O_3 response to enhanced combustion-related emissions is more complex over regions such as South America and sub-equatorial Africa when emissions of hydrocarbons such as acetaldehyde, acetone, and formaldehyde are considered in addition to emissions of NO_x. In response to the changes in O_3 and OH, the modeled CO abundance with the scaled NO_x emissions decreased by about 10% over Indonesia/Australia, for example, compared to the simulation with the a priori NO_x emissions. This reduction in CO represented about 20–30% of the contribution of emissions from the Indonesian/Australian region to the total abundance of CO and suggests that neglecting the influence of NO_x emissions (and of the emission of other precursors of O_3) on the CO chemistry could contribute to a significant bias in the CO source estimates. To accurately quantify the surface emissions of CO in an inverse modeling framework, it will be necessary to properly account for the chemical coupling of the CO-O_3-NO_x-hydrocarbon chemistry.

Although the a posteriori source estimates provided a significantly improved simulation of the TES and MOPITT data, regional residual biases remained in the simulated CO distribution, indicating the need to properly characterize systematic observation and model errors (chemical and transport). The presence of these residuals also reflects the fact that the state vector was arbitrarily selected based on geopolitical boundaries instead of the spatio-temporal resolution and precision of the data. Ideally, the inversion should be conducted at the highest resolution possible, given the information content of the observations. Our results suggest that reconciling the discrepancies between top-down source estimates will likely require obtaining more information on the sources by optimally combining boundary layer measurements of CO with TES and MOPITT data, along with observations of other tracers such as NO_2, which have similar sources as CO, in a time dependent multi-species inversion framework.

Edited by: I. Aben

References

Arellano, A. F., Kasibhatla, P. S., Giglio, L., van der Werf, G., and Randerson, J. T.: Top-down estimates of global CO sources using MOPITT Measurements, Geophys. Res. Lett., 31, L01104, doi:10.1029/2003GL018609, 2004.

Arellano, A. F., Kasibhatla, P. S., Giglio, L., van der Werf, G., Randerson, J. T., and Collatz, G. J.: Time-dependent inversion estimates of global biomass-burning CO emissions using Measurement of Pollution in the Troposphere (MOPITT) measurements, J. Geophys. Res., 111, D09303, doi:10.1029/2005JD006613, 2006.

Arellano Jr., A. F. and Hess, P. G.: Sensitivity of top-down estimates of CO sources to GCTM transport, Geophys. Res. Lett., 33, L21807, doi:10.1029/2006GL027371, 2006.

Beer, R., Glavich, T. A., and Rider, D. M.: Tropospheric emission spectrometer for the Earth Observing System's Aura satellite, Appl. Optics, 40, 2356–2367, 2001.

Bergamaschi, P., Hein, R., Heimann, M., and Crutzen, P. J.: Inverse modeling of the global CO cycle: 1. Inversion of CO mixing ratios, J. Geophys. Res., 105, 1909–1927, 2000a.

Bergamaschi, P., Hein, R., Heimann, M., and Crutzen, P. J.: Inverse modeling of the global CO cycle: 2. Inversion of $^{13}C/^{12}C$ and $^{18}O/^{16}O$ isotope ratios, J. Geophys. Res., 105, 1929–1945, 2000b.

Bey, I., Jacob, D. J., Yantosca, R. M., Logan, J. A., Field, B. D., Fiore, A. M., Li, Q., Liu, H., Mickley, L. J., and Schultz, M. G.: Global modeling of tropospheric chemistry with assimilated meteorology: Model description and evaluation, J. Geophys. Res., 106, 23073–23095, 2001.

Bowman, K. W., Rodgers, C. D., Kulawik, S. S., Worden, J., Sarkissian, E., Osterman, G., Steck, T., Luo, M., Eldering, A., Shephard, M., Worden, H., Lampel, M., Clough, S., Brown, P., Rinsland, C., Gunson, M., and Beer, R.: Tropospheric Emission Spectrometer: Retrieval method and error analysis, IEEE T. Geosci. Remote, 44, 1297–1306, 2006.

Bowman, K. W., Jones, D. B. A., Logan, J. A., Worden, H., Boersma, F., Chang, R., Kulawik, S., Osterman, G., Hamer, P., and Worden, J.: The zonal structure of tropical O_3 and CO as observed by the Tropospheric Emission Spectrometer in November 2004 – Part 2: Impact of surface emissions on O_3 and its precursors, Atmos. Chem. Phys., 9, 3563–3582, 2009, http://www.atmos-chem-phys.net/9/3563/2009/.

Deeter, M. N., Emmons, L. K., Francis, G. L., Edwards, D. P., Gille, J. C., Warner, J. X., Khattatov, B., Ziskin, D., Lamarque, J.-F., Ho, S.-P., Yudin, V., Attie, J.-L., Packman, D., Chen, J., Mao, D., and Drummond, J. R.: Operational carbon monoxide retrieval algorithm and selected results from the MOPITT instrument, J. Geophys. Res., 108(D14), 4399, doi:10.1029/2002JD003186, 2003.

Drummond, J. R. and Mand, G. S.: The Measurement of Pollution in the Troposphere (MOPITT) instrument: Overall performance and calibration requirements, J. Atmos. Ocean. Tech., 13, 314–320, 1996.

Duncan, B. N., Martin, R. V., Staudt, A. C., Yevich, R., and Logan, J. A.: Interannual and seasonal variability of biomass burning emissions constrained by satellite observations, J. Geophys. Res., 108(D2), 4040, doi:10.1029/2002JD002378, 2003.

Duncan, B. N., Logan, J. A., Bey, I., Megretskaia, I. A., Yantosca, R. M., Novelli, P. C., Jones, N. B., and Rinsland, C. P.:

The global budget of CO, 1988–1997: source estimates and validation with a global model, J. Geophys. Res., 112, D22301, doi:10.1029/2007JD008459, 2007.

Emmons, L. K., Deeter, M. N., Gille, J. C., et al.: Validation of Measurements of Pollution in the Troposphere (MOPITT) CO retrievals with aircraft in situ profiles, J. Geophys. Res., 109(D3), D03309, doi:10.1029/2003JD004101, 2004.

Emmons, L. K., Pfister, G. G., Edwards, D. P., Gille, J. C., Sachse, G., Blake, D., Wofsy, S., Gerbig, C., Matross, D., and Nedelec, P.: Measurements of Pollution in the Troposphere (MOPITT) validation exercises during summer 2004 field campaigns over North America, J. Geophys. Res., 112, D12S02, doi:10.1029/2006JD007833, 2007.

Evans, M. J. and Jacob, D. J.: Impact of new laboratory studies of N_2O_5 hydrolysis on global model budgets of tropospheric nitrogen oxides, ozone, and OH, Geophys. Res. Lett., 32, L09813, doi:10.1029/2005GL022469, 2005.

Gloudemans, A. M. S., Krol, M. C., Meirink, J. F., de Laat, A. T. J., van der Werf, G. R., Schrijver, H., van den Broek, M. M. P., and Aben, I.: Evidence for long-range transport of carbon monoxide in the Southern Hemisphere from SCIAMACHY observations, Geophys. Res. Lett., 33, L16807, doi:10.1029/2006GL026804, 2006.

Heald, C. L., Jacob, D. J., Jones, D. B. A., Palmer, P. I., Logan, J. A., Streets, D. G., Sachse, G. W., Gille, J. C., Hoffman, R. N., and Nehrkorn, T.: Comparative inverse analysis of satellite (MOPITT) and aircraft (TRACE-P) observations to estimate Asian sources of carbon monoxide, J. Geophys. Res., 109, D23306, doi:10.1029/2004JD005185, 2004.

Hudman, R. C., Jacob, D. J., Turquety, S., et al.: Surface and lightning sources of nitrogen oxides over the United States: magnitudes, chemical evolution, and outflow, J. Geophys. Res., 112, D12S05, doi:10.1029/2006JD007912, 2007.

Hudman, R. C., Murray, L. T., Jacob, D. J., Millet, D. B., Turquety, S., Wu, S., Blake, D. R., Goldstein, A. H., Holloway, J., and Sachse, G. W.: Biogenic versus anthropogenic sources of CO in the United States, Geophys. Res. Lett., 35, L04801, doi:10.1029/2007GL032393, 2008.

Jones, D. B. A., Bowman, K. W., Palmer, P. I., Worden, J. R., Jacob, D. J., Hoffman, R. N., Bey, I., and Yantosca, R. M.: Potential of observations from the Tropospheric Emission Spectrometer to constrain continental sources of carbon monoxide, J. Geophys. Res., 108(D24), 4789, doi:10.1029/2003JD003702, 2003.

Kasibhatla, P., Arellano, A., Logan, J. A., Palmer, P. I. and Novelli, P.: Top-down estimate of a large source of atmospheric carbon monoxide associated with fuel combustion in Asia, Geophys. Res. Lett., 29(19), 1900, doi:10.1029/2002GL015581, 2002.

Kopacz, M., Jacob, D. J., Henze, D. K., Heald, C. L., Streets, D. G., and Zhang, Q.: Comparison of adjoint and analytical Bayesian inversion methods for constraining Asian sources of carbon monoxide using satellite (MOPITT) measurements of CO columns, J. Geophys. Res., 114, D04305, doi:10.1029/2007JD009264, 2009.

Liu, J., Drummond, J. R., Jones, D. B. A., Cao, Z., Bremer, H., Kar, J., Zou, J., Nichitiu, F., and Gille, J. C.: MOPITT Observations of Large Horizontal Gradients in Atmospheric CO at the Synoptic Scale, J. Geophys. Res., 111, D02306, doi:10.1029/2005JD006076, 2006.

Luo, M., Rinsland, C. P., Rodgers, C. D., Logan, J. A., Worden, H., Kulawik, S., Eldering, A., Goldman, A., Shephard, M. W., Gunson, M., and Lampel, M.: Comparison of carbon monoxide measurements by TES and MOPITT – the influence of et al data and instrument characteristics on nadir atmospheric species retrievals, J. Geophys. Res., 112, D09303, doi:101029/2006JD007663, 2007a.

Luo, M., Rinsland, C., Fisher, B., Sachse, G., Diskin, G., Logan, J. A., Worden, H., Kulawik, S., Osterman, G., Eldering, A., Herman, R., and Shephard, M.: TES carbon monoxide validation with DACOM aircraft measurements during INTEX-B 2006, J. Geophys. Res., 112, D24S48, doi:10.1029/2007JD008803, 2007b.

Müller, J.-F. and Stavrakou, T.: Inversion of CO and NO_x emissions using the adjoint of the IMAGES model, Atmos. Chem. Phys., 5, 1157–1186, 2005,
http://www.atmos-chem-phys.net/5/1157/2005/.

Park, R. J., Jacob, D. J., Palmer, P. I., Clarke, A. D., Weber, R. J., Zondlo, M. A., Eisele, F. L., Bandy, A. R., Thornton, D. C., Sachse, G. W., and Bond, T. C.: Export efficiency of black carbon aerosol in continental outflow: global implications, J. Geophys. Res., 110, D11205, doi:10.1029/2004JD005432, 2005.

Palmer, P. I., Suntharalingham, P., Jones, D. B. A., Jacob, D. J., Streets, D. G., Fu, Q., Vay, S., and Sachse, G. W.: Using CO_2:CO correlations to improve inverse analyses of carbon fluxes, J. Geophys. Res., 111, D12318, doi:10.1029/2005JD006697, 2006.

Palmer, P. I., Jacob, D. J., Jones, D. B. A., Heald, C. L., Yantosca, R. M., Logan, J. A., Sachse, G. W., and Streets, D. G.: Inverting for emissions of carbon monoxide from Asia using aircraft observations over the western Pacific, J. Geophys. Res., 108, 8825, doi:10.1029/2002JD003176, 2003.

Parish, D. F. and Derber, J. C.: The National Meteorological Center's spectral statistical interpolation analysis system, Mon. Weather Rev., 120, 1747–1763, 1992.

Pétron, G., Granier, C., Khattatov, B., Lamarque, J.-F., Yudin, V., Muller, J.-F., and Gille, J. C.: Inverse modeling of carbon monoxide surface emissions using CMDL network observations, J. Geophys. Res., 107, 4761, doi:10.1029/2001JD002049, 2002.

Rodgers, C. D.: Inverse Methods for Atmospheric Sounding: Theory and Practice, World Scientific, Singapore, 2000.

Stavrakou, T. and Müller, J.-F.: Grid-based versus big region approach for inverting CO emissions using Measurement of Pollution in the Troposphere (MOPITT) data, J. Geophys. Res., 111, D15304, doi:10.1029/2005JD006896, 2006.

Suntharalingam, P. P., Jacob, D. J., Palmer, P. I., Logan, J. A., Yantosca, R. M., Xiao, Y., Evans, M. J., Streets, D., Vay, S. A., and Sachse, G.: Improved quantification of Chinese carbon fluxes using CO_2/CO correlations in Asian outflow, J. Geophys. Res., 109, D18S18, doi:10.1029/2003JD004362, 2004.

van der Werf, G. R., Randerson, J. T., Collatz, G. J., Giglio, L., Kasibhatla, P. S., Arellano, A. F., Olsen, S. C., and Kasischke, E. S.: Continental-scale partitioning of fire emissions during the 1997 to 2001 El Nino/La Nina period, Science, 303, 5654, 73–76, 2004.

van der Werf, G. R., Randerson, J. T., Giglio, L., Collatz, G. J., Kasibhatla, P. S., and Arellano Jr., A. F.: Interannual variability in global biomass burning emissions from 1997 to 2004, Atmos. Chem. Phys., 6, 3423–3441, 2006,
http://www.atmos-chem-phys.net/6/3423/2006/.

Wang, Y. X., McElroy, M. B., Martin, R. V., Streets, D. G., Zhang, Q., and Fu, T.-M.: Seasonal variability of NO$_x$ emissions over east China constrained by satellite observations: Implications for combustion and microbial sources, J. Geophys. Res., 112, D06301, doi:10.1029/2006JD007538, 2007.

Worden, H. M., Logan, J., Worden, J. R., Beer, R., Bowman, K., Clough, S. A., Eldering, A., Fisher, B., Gunson, M. R., Herman, R. L., Kulawik, S. S., Lampel, M. C., Luo, M., Megretskaia, I. A., Osterman, G. B., and Shephard, M. W.: Comparisons of Tropospheric Emission Spectrometer (TES) ozone profiles to ozonesodes: methods and initial results, J. Geophys. Res., 112, D03309, doi:10.1029/2006JD007258, 2007.

Yevich, R. and Logan, J. A.: An assesment of biofuel use and burning of agricultural waste in the developing world, Global Biogeochem. Cy., 17(4), 1095, doi:10.1029/2002GB001952, 2003.